Research Article

Integrative Approach for Early Cataract Detection using Whale Optimized Convolutional Gated Recurrent Neuronet

Mrs. S.B. Saleema Parvin[1], Dr. S. Ismail Kalilulah[2]

[1]PhD Research Scholar, Faculty of Computer Applications, Dr. MGR Educational and Research Institute, Maduravoyal, Chennai,
Mail ID: saleemaparvin.s.b@jbascollege.edu.in

[2]Professor, Department of Computer Science and Engineering, Dr. MGR Educational and Research Institute, Maduravoyal, Chennai - 600095,
Mail ID: ismailkalilulah.cse@drmgrdu.ac.in
ismailkalilulah125@gmail.com

ARTICLE INFO	ABSTRACT
	Background: The development and visual impairment caused by cataracts, the primary cause of blindness in many other nations, must be addressed with regular screening and prompt treatment. Vision distortion is a typical result of eye illnesses such as cataracts. The greatest method of reducing the risk and preventing blindness is early and accurate cataract identification. Research attention has recently been drawn to artificial intelligence-based cataract detection methods. **Purpose:** The research enhances diagnosis accuracy and care timeliness, improving clinical outcomes for patients with detected cataract illness. **Methods:** The Kaggle Cataract Disease detection dataset is utilized in the research for detection purposes. Resize and color adjustment are used to improve the quality of the images and make feature extraction smoother afterward. Global Contrast Normalization (GCN) is used during the preprocessing step. Utilize the Oriented FAST and rotated BRIEF (ORB) algorithm, and Efficient Net to extract features in images of cataract illness, ensuring a reliable and efficient method for identifying distinguishing characteristics. The research proposed a Whale Optimized Convolutional Gated Recurrent NeuroNet (WOCGRN) to improve diagnosis accuracy and care timeliness, thereby improving clinical outcomes for cataract patients. This novel model combines the spatial learning power of Convolutional Neural Nets (CNNs) with Whale Optimization's Gated Recurrent Unit layers to fine-tune the research model. **Result:** Furthermore, the model has been designed to concentrate on symmetrical areas of interest within images, enhancing its sensitivity to microscopic structural alterations linked to cataract disease. Using the Python tool and comparative analysis demonstrates that the model outperforms existing methods. Compared to previous models, the proposed WOCGRN model achieves superior performance metrics: 99.49% accuracy, 99.00% precision, 98.00% recall, 98.00% F1 score, 97% sensitivity, and 96% specificity. **Conclusion:** These results underscore the potential of integrative approaches in developing a robust diagnostic tool for the early detection of cataract diseases, ultimately contributing to improved patient outcomes. **Keywords:** Cataract Diseases (CD), Global Contrast Normalization (GCN), Oriented FAST and rotated BRIEF (ORB), Whale Optimized Convolutional Gated Recurrent NeuroNet (WOCGRN).

I.INTRODUCTION

A cataract can develop from protein accumulation on the lens of the eyes. This will obscure the lens and stop light from traveling through it, which will impair vision**[1]**. These changes often begin after the age of 40 and are a normal part of aging. By the time they are 80, more than half of all Americans will have undergone cataract surgery or have cataracts**[2]**. **Figure 1** shows the affected cataract eye.
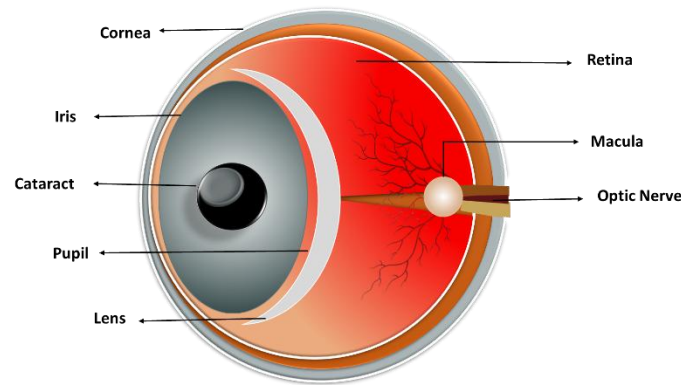
Figure 1: Cataract eye

A common eye ailment that frequently manifests before the age of sixty is cataract. Diabetes, trauma, medications, and other health issues can all be associated with early cataract development**[3]**. A traumatic eye injury, such as being struck by a ball, poked or wounded by a sharp instrument, being exposed to UV radiation, receiving ionizing radiation therapy for an eye tumour, getting chemicals in the eye, or suffering electrical damage to any part of the body, is the most frequent cause among young individuals. Cataracts develop gradually, often starting with subtle vision changes that can go unnoticed at first **[4]**.

1.1   Early cataract symptoms

Cataracts are a common eye condition characterized by the clouding of the lens, which can significantly impair vision. In their early stages, cataracts can produce subtle symptoms that can easily be overlooked or attributed to normal aging. However, recognizing these symptoms is crucial for timely intervention and effective management. One of the initial signs of early cataracts is the alteration in color perception; individuals often report that colors appear faded or yellowed, diminishing the vibrancy of their surroundings **[5]**. As the condition progresses, increased sensitivity to glare becomes apparent, particularly when driving at night, where bright headlights can create discomfort and visual disturbances. Another notable symptom is double vision in one eye, which occurs due to irregularities in the lens, causing light to scatter and resulting in a perception of seeing two images**[6]**. Additionally, those affected can find themselves needing more light for close work, such as reading or sewing, as the clouding of the lens decreases the amount of light that reaches the retina. Finally, blurred vision, often experienced in one eye, can manifest early on and worsen over time, leading to a significant impact on daily activities. Understanding these early symptoms is essential for individuals to seek prompt evaluation and treatment, ultimately preserving their quality of vision and overall quality of life.

1.2 Causes of Early Cataracts

Early cataract is a disorder in which the lens of the eye clouds early in life, usually before the age of 50**[7]**. If left untreated, symptoms like blurred vision, increased light glare, and difficulty seeing at night can have a major negative impact on daily activities and quality of life. The illustration of causes is shown in **Figure 2.**
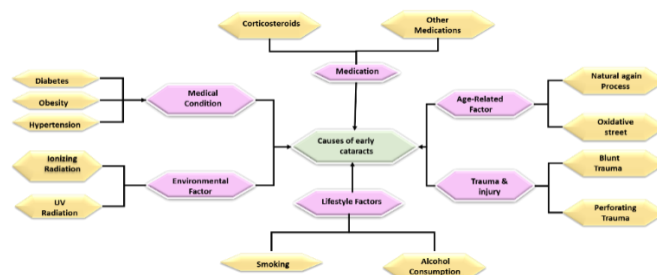

Figure 2: Causes of early cataract

1.3   Research objective

The study improves diagnosis accuracy and care timeliness, leading to improved clinical outcomes for patients with detected cataract illness.

The remainder of the research:Section 2 contains the study's review of the literature, and **Section 3** illustrates the methodology. The results of the study are presented in **Section 4**. The conclusion is established in **Section 5.**

II.LITERATUR REVIEW

Table 1 summarizes the literature on various types of cataracts, detailing the year of publication, the datasetused, research objectives, methodologies employed, advantages, and identified limitations of each study, providing a comprehensive overview of the current state of research in the field.

Table 1: Overview of various articles related to cataract disease

REFERENCE & YEAR	OBJECTIVE	DATA	PROPOSED METHOD	ADVANTAGES	DRAWBACKS
[8], 2024	To enhance early and preciserecognition of the cataracts as well as glaucoma to reduce the risk of blindness.	The experiments utilized publicly available datasets containing images of cataracts and normal eyes, and glaucoma and normal eyes.	The study employed MobileNetV1 along withMobileNetV2that are optimized architectures for lightweight deep neural networks using the depth-wise separable convolutions.	The suggestedapproach achieved the highest precision compared to the other approaches.	Study is limited by the use of publicly available datasets, which cannot represent all variations of cataract and glaucoma cases.
[9], 2024	To develop a reliable model for classifying eye diseases to advance medical science and increase patient outcomes.	Fundus images of various eye diseases, including cataracts, glaucoma, and diabetic retinopathy.	BayeSVM500, a Support Vector Machine (SVM) classifier trained on features extracted from Efficient Net and reduced to 500 dimensions.	The methodattainedaccuracy (95.33 ± 0.60%), indicating highly accurate classification and potentially improving diagnosis speed and patient outcomes. 40 mini	The model's performance can depend on the quality and diversity of the training dataset; it cannot generalize well to unseen data.
[10], 2024	To classify fundus images into two classes: normal and cataract, enabling early detection and prevention.	Fundus images from the Kaggle repository are divided into training data, validation data, and test data.	Utilization of the EfficientNet architecture in convolutional neural networks (CNN) and comparison of various optimizers	The comparison of multiple optimizers provides insights into their effectiveness, aiding future research in selecting the best optimization strategy for similar tasks.	The model's performance can be influenced by the limited size of the training dataset, potentially affecting generalizability.

[11], 2024	To detect, recognize, and classify cataracts using deep learning (DL) models applied to retinal fundus color images, intended for early detection and treatment.	A dataset of 400 colourimages has been classified into 300 normal images and 100 cataract images.	Utilization ofCNN models, GoogleNet, ResNet101, and DenseNet201applied in three scenarios.	The model's potential for early detection and classification of cataracts weredemonstrated through performance metrics evaluation, enhancing its reliability and improving eye health.	Not explicitly mentioned in the abstract, but potential limitations include dependency on the quality of the dataset and variability in image capture conditions.
[12], 2024	To classify congenital cataracts for personalized treatment and to predict visual outcomes.	Medical records of 164 children with congenital cataracts, involving 299 eyes	Hierarchical cluster analysis to identify different clusters based on ocular features	Identified two clusters with different visual outcomes, aiding in treatment decisions.	The study is retrospective, which can introduce biases.
[13], 2024	To enhance the accuracy of cataract diagnosis.	Fundus images of normal eyes and cataracts from Kaggle.	SVM and a Harmony Search algorithm.	Improved computational efficiency through better exploration of the search space.	Potential issues with the dataset's quality and diversity
[14], 2024	To develop an AI-based network for high-precision classification and grading of cataracts using fundus images	1,340 color fundus images from 875 participants from the Beijing Eye Study 2011.	Developed a DualStream Cataract Evaluation Network (DCEN) for simultaneous cataract type classification and severity grading.	Simultaneous classification and grading streamline assessments.	Limited generalizabil ity due to data from a single location (Beijing).
[15], 2024	To evaluate outcomes related to fusing visual characteristics of the left as well as right eye cataract features for improved classification of ocular disorders.	Ocular Disease Intelligent Recognition (ODIR5k) dataset.	Introduced CataractNetDetect, a multi-label DL classification system that fuses the characteristicillustra tions from pairs of fundus images using architectures.	Streamlines the diagnostic process, allowing for quicker and more efficient evaluations of ocular disorders.	The research used an exact dataset, which can affect its generalizatio n to other populations.

III.METHODOLOGY

To improve the diagnosis of cataract disease, the Whale Optimized Convolutional Gated Recurrent NeuroNet (WOCGRN) is utilized in the suggested technique. The temporal processing strengths of Gated Recurrent Unit (GRU)

layers are combined with the spatial learning powers of CNN in the present novel model. To optimize the GRU parameters and ensure effective model fine-tuning, the Whale Optimization Algorithm is utilized. Through the integration of these advancededge methods, WOCGRN seeks to enhance patient care timeliness as well as diagnostic precision. The ultimate goal of this strategy is to improve clinical results and the way cataract illness is managed in general. **Figure 3** depicts the overall block diagram.
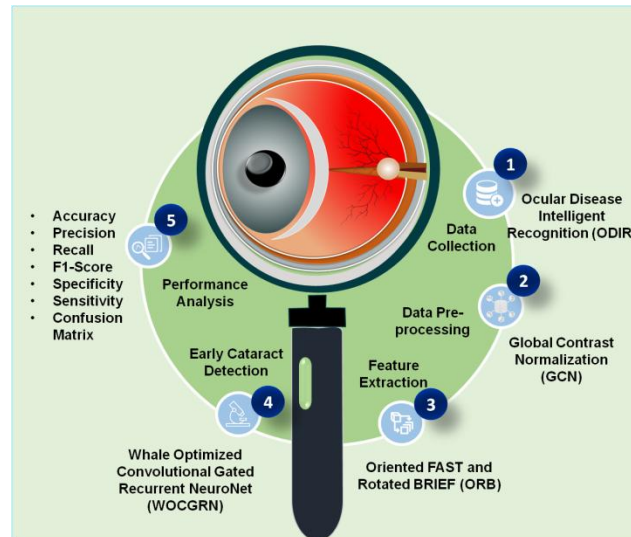

Figure 3: Overall Methodological design

3.1 Dataset

Research gathers ocular disease intelligence recognition (ODIR) (https://www.kaggle.com/datasets/andrewmvd/ocular-disease-recognition-odir5k?select=ODIR-5K) dataset from Kaggle, it's a database of 5,000 patients, containing age, colour fundus images, and doctors' diagnostic keywords. It represents real-life patient information from hospitals and medical centers using cameras like Canon, zeiss, and kowa, resulting in varied image resolutions. The dataset represents a real-life set of patient information**. Figure 4** illustrates the sample images of data.
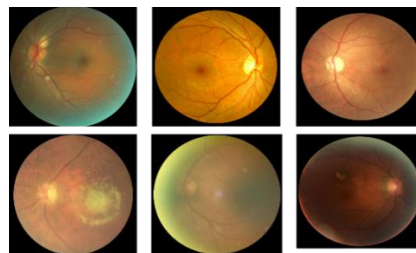

Figure 4: Example images in the database

3.2 Data Pre-processing

Two crucial methods used to improve image quality are resizing and color modification, which allow for more fluid feature extraction in later stages. One essential pre-processing procedure that helps standardize image contrast and provide similar visual qualities across different images is called global contrast normalization, or GCN. By using these techniques, the images' overall clarity and detail are enhanced, which eventually leads to more accurate analysis and interpretation. When combined, these pre-processing methods provide a strong basis for machine learning (ML) and image processing applications.

3.2.1 Histogram Equalization (HE)

Splitting pixel intensity values improves image contrast and makes features more visible in both dark and bright areas. This process is known as HE. This technique improves the visibility of details in images taken in dimly lit environments. HE enhances the contrast in images, making subtle differences in consistencyand quality more apparent. **Figure 5** represents the quality image of pre-processed HE. By normalizing brightness and contrast, this

pre-processing step increases the accuracy of feature extraction and classification, allowing for the distinction of affected.**Eq. (1-3)** represents the HE.

$$l = 0,1, \ldots . K - 1 \qquad \text{(eq. 1)}$$

$$d(w) = \sum_{i=0}^{l} o(W_i) \qquad \text{(eq. 2)}$$

$$e(w) = W_0 + (W_{K-1} - W_0)d(w) \qquad \text{(eq. 3)}$$

In the equations, l represents the possible intensity levels of the image, $d(w)$ denotes the cumulative distribution function for the intensity levels, and $e(W)$ signifies the equalized intensity value. The high performance of the HE to enhance the image contrast due to the dynamic range expansion, which can be easily understood by the image output of the HE, is as shown in **Eq. (4 & 5).**

$$Z = e(W) \qquad \text{(eq. 4)}$$

$$\{e(W(j,i))|\forall W(j,i) \in W\} \qquad \text{(eq. 5)}$$

$Z$is the enhanced output image after HE, and W represents the original image intensity values at pixel locations (j,i).
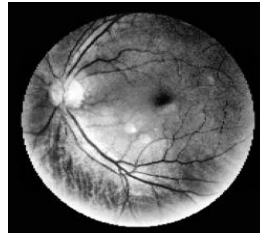

Figure 5: After using histogram equalization (HE)

3.2.2 Global Contrast Normalization (GCN)

To provide a consistent visual representation, GCN modifies the mean and variance across pixel intensities to normalize the contrast of images. By minimizing lighting-related differences, this approach makes it possible to compare and analyse images more effectively for ML tasks. GCN is crucial for improving the quality of medical images, particularly in ODIR for cataracts. GCN enhances image contrast, making important characteristics like cataract opacities easier to see**(Eq. 6)**. It also standardizes image intensity levels, reducing unpredictability caused by uneven lighting or camera settings. This enhances the overall image quality, making it easier to compare samples and identify signs of cataract existence or severity.

$$I_{normalized}(x,y) = \frac{I(x,y) - \mu}{\mu} . \alpha + \beta \qquad \text{(eq. 6)}$$

$I(x,y)$is the original pixel intensity at coordinates (x,y), μ is the mean intensity of the image, σ is the standard deviation of the image intensities, α is a scaling factor that controls the contrast, and β is a bias that can be adjusted to shift the intensity values.**Figure 6** illustrates after using normalized data.
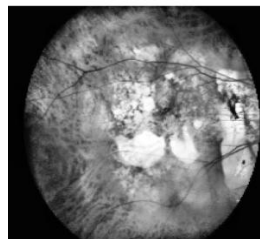

Figure 6: After using GCN

3.3 Feature extraction using oriented fast and rotated brief (ORB) algorithm

Rotating BRIEF and FAST algorithms are well-liked due to their good performance and low time requirements. Real-time FAST detector finds keypoints that meet specific visual qualities; ORB uses Harris corner measure to sort the keypoints into order. To find more than N important locations, ORB sets a low threshold in the first phase. The Harris

measure is then used to order the points and select the top$M$. The FAST detector uses a scale pyramid to measure and filter FAST characteristics at each level rather than creating multi-scale features. ORB determines corner orientation using the intensity centroid approach, which based an orientation on the intensity of a corner. Rosin computes patch moments using **Eq.(7)**.

$$n_{or} = \sum_{w,z} w^o z^r J(w,z)$$ (eq. 7)

Next, the centroid is going to be depicted in **Eq. (8)**:

$$D = \left(\frac{n_{10}}{n_{00}}, \frac{n_{01}}{n_{00}} \right)$$ (eq. 8)

$(\overrightarrow{OD})$ is the possible vector that forms from the centroid (D) to the center of the corner (p), and the orientation of this patch is represented in **Eq. (9)**:

$$\theta = \text{atan} 2(n_{01}, n_{10})$$ (eq. 9)

Where the quadrant aware form of atan is (($b\,tan\,2$)). Within the specified circular zone, the moments are monitored in the w and z directions to improve rotation invariance. The BRIEF descriptor is a faster, less memory-intensive, and more efficient image comparison method compared to vector-based feature descriptors. It uses binary tests across pixels in a smoothed image region and prioritizes the search of hierarchical clustering trees, even without GPU acceleration. ORB can match signature images by over two orders of magnitude. The descriptor also generates a bitstring description of image patches and effectively steers key pointalignment. As demonstrated in **Eq. 10**, a feature set at (w_j, z_j) may be represented as a 2 ×mmatrix for m binary tests.

$$T = \begin{pmatrix} w_1 \dots w_m \\ z_1 \dots z_m \end{pmatrix}$$ (eq. 10)

The steered version (T_θ)of (T)is calculated as **Eq. (11)**using the orientation of the patch (θ) and the corresponding rotationmatrix(Q^θ).

$$T_\theta = Q^\theta T$$ (eq. 11)

Then **Eq. (12)**is the guided BRIEF operator:

$$h_m(O, \theta) = e_m(O)(w_j, z_j) \in T_\theta$$ (eq. 12)

The binary descriptor ORB encodes patch information as a binary string using image intensity comparisons, which is a faster method than the gradient histograms with merely the hamming separation, ORB can pair up two photos in a single request. **Figure 7** shows an example of extracting features from data.
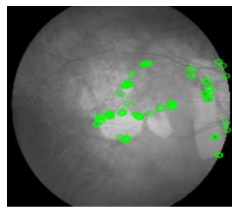

Figure 7: After extracted features

3.4 Whale Optimized Convolutional Gated Recurrent NeuroNet (WOCGRN)

The proposed technique uses the WOCGRN to enhance cataract diagnosis. This model combines the temporal processing strengths of GRU layers with the spatial learning powers of CNN, aiming to improve patient care timeliness and diagnostic precision.

3.4.1 Convolutional Neural Network (CNN)

A CNN model is used to improve the accuracy of early cataract classification. Through the use of advanced DL techniques, the model can interpret and classify early cataract detectionwith effectiveness. This method facilitates real-time applications by increasing identification speed and reliability. The CNN approach, which consists of a fully SoftMax Layer, connected layer, convolutional layer, andpooling layer, has been designed to identify early cataract detection.

i.   Convolutional layer

It contains feature maps, such as depth slices along with every feature map including collections of neurons. **Eq. (13)**provides the outcome of the convolution process in the convolutional layer. Where E indicates the kernel (filter) dimension, n denotes feature maps, A represents bias, and X_i indicates kernel weight. The convolutional layer outcome is represented asz_j^k, where j signifies the jth feature map within a layer designated by$k$.

$$z_j^k = A_j^1 + \sum_{i=1}^{n_1(1-1)} E_{j,i^k} \times X_i^{(k-1)} \qquad \text{(eq. 13)}$$

ii.   Pooling layer

To reduce the quantity of variables and network computations, the pooling layer is typically utilized between the convolutional layers. As a consequence, using the sub-sampling function, the input dimension is reduced in every depth division, preventing over-fitting during network training. Since the input spatial dimension is reduced through the pooling procedure, the depth size has not altered. The output height and width are accomplished in the pooling layer using **Eq. (14&15)**. Where X_1 represents the input's width, G_1 represents the input's height, T denotes the stride dimension, and E indicates the kernel dimension.

$$X_2 = \left(\frac{X_1+E}{T}\right) + 1 \qquad \text{(eq. 14)}$$

$$G_2 = \left(\frac{G_1+E}{T}\right) + 1 \qquad \text{(eq. 15)}$$

iii.   Fully connected layer

The final layer of the framework represents a fully connected layer. In the fully connected layer, every neuron in that layer has been connected with every neuron in the preceding layer. **Eq. (16)** provides the fully connected procedures, with k and $(k-1)$ representing fully linked layers. The jth unit in layer k represents the outcome of the final fully linkedz_j^k. Layer k contains feature maps of $n_1^{(k-1)}$ through $n_2^{(k-1)} \times n_3^{(k-1)}$dimensions that are specified as inputs. $X_{j,i,q,t}^k$Represent the weighted relations of the jth unit in layer k as well as Z_j, which is indicated as the ith layer unit$(k-1)$ in the (q,t) position.

$$z_j^k = e(z_j^k) \ with z_j^k = \sum_{i=1}^{n_1^{(k-1)}} \sum_{q=1}^{n_2^{(k-1)}} \sum_{t=1}^{n_3^{(k-1)}} X_{j,i,q,t}^k (z_i^{k-1})_{q,t} \qquad \text{(eq. 16)}$$

iv.   SoftMax layer

In general, during the final layer of the framework, the SoftMax function has been employed to determine the possibility of every ground truth label of outcomes from0 to 1, and the value of the outcome is converted to a perceptible value. **Eq. (17)**defines the SoftMax function. In this equation, l denotes the size of randomized values (y), which are transformed into significant values from zero to one through the softmax function $e(y)$.

$$e(y)_j = \frac{f^{y_i}}{\sum_{l=1}^{l} f^{y_l}} \ for \ i = 1, \dots, l \qquad \text{(eq. 17)}$$

CNN features detect early injury cataracts, anomalies, and early warning symptoms, improving data management and enabling prompt intervention and personalized rehabilitation strategies, thereby improving early cataract efficiency.

3.4.2 Gated recurrent unit (GRU)

GRUs utilize gating mechanisms to control the flow of sequential data, making them ideal for tasks like language modeling, timeseries prediction, and video analysis that require an understanding of sequence and context over time. The GRU techniqueissimplerand quicker than traditional LSTMsince it combines the input and forgetting gates into a single update gate. Large datasets can benefit greatly from this, as it saves time and reduces performance disparities. Using different gates, the LSTM and GRU models both maintain important characteristics, making sure they hold up over extended transmissions. **Eq. (18)**can be used to determine the new state at time$s$.

$$v_s = (1 - y_s) \circ v_{s-1} + b_h \circ \tilde{v}_s \qquad \text{(eq. 18)}$$

Where b_h is the advance gate, v_s is the presentapplicant state with a fresh set of data, v_{s-1} is the prior GRU state, and v_s is the innovative GRU state. By modifying the value of b_h, the update gate controls how prior data is incorporated into the present state. A higher number denotes a larger integration of earlier data. Its main purpose is to strike a balance between adding new information and preserving older information. **Eq. (19)**defines the procedure for upgrading the update gate.

$$b_h = \delta(X_y w_s + Q_y v_{s-1} + b_g) \tag{eq. 19}$$

Where b_h is biasing, X_y is the apprise gate weights, Q_y is the update gate weights at time $s - 1$, and $w_s$is the data vector at time s. **Eq. (20)**is used to determine the current candidate state.

$$\tilde{v}_s = \tanh(X_y w_s + q_y \circ Q_y v_{s-1}) \, b_y \tag{eq. 20}$$

Additionally, q_y denotes a reorganized gate at time s. The GRU network extends unidirectional networks, allowing hidden-to-hidden connections to flow in the opposite temporal sequence, improving models' understanding and data utilization from both directions.

3.4.3 Whale optimization (WO)

Study discusses the use of WO for early detection of cataracts.The WO model intends to maximize problem-solving efficiency by leveraging the concepts of the Whale Optimization Algorithm (WOA). This model effectively searches the solution space to identify optimal solutions by emulating the social behaviours of humpback whales. The algorithm is inspired by the humpback whale bubblenet feeding method, which involves encircling prey and attacking, resulting in both exploration and exploitation phases during the optimization process. This approach has proven effective in finding optimal parameters for complex models. The goal of this optimization strategy is faster convergence, which accelerates the solution-finding process. It is particularly suitable for challenging optimization problems, as it emphasizes increasing accuracy while minimizing computational costs. The WO model's ultimate goal is to deliver trustworthy outcomes for a wide range of applications. Assume the search space has N dimensions and B search agents are in the swarm.In the search space, each search agent is represented as$\{t_{h1}, t_{h2}, t_{h3} \ldots t_{hm}\}$, where$u = \{1,2,3\ldots B\}$; Swarm $=\{A_1, A_2, A_3 \ldots A_m\}$. The three steps of the whale optimization method are as follows:

- encompassing prey
- Phase of exploitation
- investigation stage

The first thing the search agents do is locate the best option and circle it. After that, the objective function is utilized to establish the current best candidate answer. The best-realized response, which is currently the best candidate, is seen to be a close substitute for the ideal answer. Once the most suitable option has been identified, additional potential options or searchers attempt to improve their positions in favor of the best candidate solution. The search agents' positions are updated following **Eq. (21 & 22)**.

$$X = |S. Q^*(a) - Q(a)| \tag{eq. 21}$$

$$Q(a + 1) = S. Q^*(s) - VX \tag{eq. 22}$$

A stand for V and X are vectors, the current iteration number, and with equal coefficients. Using the symbol $||$ indicates that the values used are absolute. Q designates the position vector of the current search agent and represents the position vector of the best candidate solution. The importance of $V \text{ and } X$ are determined using **Eq. (23& 24)**, respectively.

$$V = 2. v. m. v \tag{eq. 23}$$

$$S = 2. me \tag{eq. 24}$$

When m is an arbitrary path with a range of [0, 1], the components linearly lowered from 2 to 0 throughout execution.

The exploitation phase immediately follows the grade of encircling the victim. The strategies of humpback whales served as the inspiration for this stage. The name bubblenet also knows the mechanism. Two methods are taken into consideration for modeling the humpback whales' bubble net behavior:

- Consequently, V's value is determined randomly within the choice. The value declines evenly over the repetitions, from 0 to1.
- The positionupdating spiral mechanism estimates how far apart the present place and the search agency are the ideal location of a searching agent. A revolving equation is next. Corresponds to the humpback whales' spiral-shaped movement. **Eq. (25)** is used to represent this movement.

$$Q(a + 1) \; = X'.d^{xw}.cos(2\pi k) + X^*(A) \hspace{3cm} (eq. 25)$$

Where a is a constant and l is a random value within the range, d indicates the separation between the ideal search agent location and the present position. The search agent's site is updated throughout this phase using both approaches. It is presumed that there is a 50% chance of choosing one of these two processes. According to, **Eq.(26)** the exploitation phase's whole operation is shown.

$$Q(a + 1) \; = \begin{cases} Q(a + 1) = Q^*(s) - V.X \; if \; o < 0.5 \\ X'.d^{ph}.cos(2\pi j) + Q^*(t) \; if \; o \geq 0.5 \end{cases} \hspace{1.5cm} (eq. 26)$$

Where [0, 1] is a range of possible numbers for o. The exploration phase, the last stage of the algorithm, involves the search agents moving randomly across the search space in pursuit of the optimal solution while updating their positions under the positions of other agents. The value of V utilized is $either \; > 1 \; or \; 1$ to shift the reference search agent; the search agents are separated. The investigation stage's theoretical model is presented by **Eq. (27 & 28).**

$$X = |S.Q_{rand} - Q| \hspace{5cm} (eq. 27)$$

$$Q(a + 1) \; = \; Q_{rand} - V.X \hspace{4.5cm} (eq. 28)$$

Enhancing performance, the WOCGRN combines the efficacious feature extraction of CNNs with the sequential data processing strength of GRUs and the efficient search capabilities of WO. Accuracy in challenging pattern recognition tasks, especially with timeseries data, is enhanced by this combination. Furthermore, by minimizing over-fitting and computational cost, the hybrid technique guarantees quicker convergence and improved generalization. **Algorithm 1** depicts the WOCGRN.

Algorithm 1:WOCGRN

Initialize the population of whales (search agents) with random positions in the solution space.
Evaluate the fitness of each whale using the objective function.
Identify the best-performing whale as the leader.
For each whale in the population:
Update position based on the leader's position (encircling prey).
If random number < 0.5 (exploitation phase):
Choose between shrinking encircling or spiral updating:
If shrinking, reduce the distance to the leader's position.
Else, use a spiral update mechanism for a new position.
Else (exploration phase):
Move randomly in the search space.
Evaluate new positions and update fitness.
If any whale outperforms the leader, update the leader.
Repeat steps for a defined number of iterations or convergence criteria.
Return the position of the best whale as the optimal solution.

IV.   PERFORMANCE ANALYSIS

4.1 Experimental Setup

An HP brand system with an Intel Core i912900 processor, an Intel Core i713700 CPU type, 3.50 GHz clock speed, 64 GB RAM, Windows 11 Home operating system, Python version 3.10.0, and a 16 MB L3 cache size is described in **Table 2**, along with the hardware and software components of the computer.

Table 2: Experimental setup

| PROCESSOR MODEL	INTEL(R) CORE(TM) I912900
Brand	HP
CPU Type	Intel Core i713700
Clock Speed	3.50 GHz
Memory (RAM)	64 GB
Operating System	Windows 11 Home
Python Version	3.10.0
L3 Cache Size	16 B

4.2 Comparative Analysis

The study improves diagnosis accuracy and care timeliness, leading to improved clinical outcomes for patients with detected cataract illness. The suggested approach is contrasted with existing approaches, including Stacking EL of 3 CNN**[16],**CNN with 2D-discrete Fourier transform (2D DFT) **[17]**, LeNet-CNN (LeNet-CNN) **[18]**,Visual Geometry Group (VGG) 19 **[19]**, and CNN with an ensemble of SVM, NB, RF (CNN+SVM+NB+RF)**[20]**.

4.2.1 Accuracy

It calculates the percentage of instances of both cataracts and non-cataracts that are properly diagnosed out of all of the cases. It displays the detection model's total efficacy. WOCGRN achieves 99.49% accuracy, outperforming models like CNN+SVM+NB+RF (97.34%), Stacking EL of 3CNN (93.97%), CNN with 2DDFT (93.10%), LeNet-CNN (96%), and VGG 19 (93.12%).**Figure 8** and **Table 3** depict the graphical and numerical outcomes of accuracy.

Table 3: Numerical outcomes of accuracy

Methods	Accuracy (%)
Stacking EL of 3CNN [16]	93.97
CNN with 2D DFT [17]	93.10
LeNet-CNN [18]	96
VGG 19 [19]	93.12
CNN+SVM+NB+RF [20]	97.34
WOCGRN [Proposed]	**99.49**
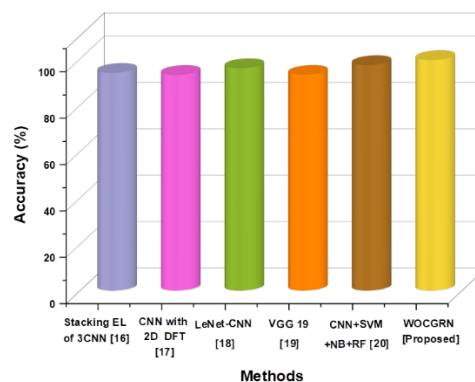
Figure 8: Graphical representation of accuracy

4.2.2 Precision

It indicates the proportion of correctly detected cataract cases (true positives) out of all cases flagged as cataracts (true positives + false positives), reflecting the model's reliability in identifying cataracts without false alarms. With a 99.00% precision, the research model surpasses Stacking EL of 3 CNN (94.20%), CNN+SVM+NB+RF (93.87%), VGG 19 (92%), and CNN with 2DDFT (93.08%).**Table 4** depicts the numerical findings of precision; **Figure 9** illustrates the graphical findings of precision.

Table 4: Numerical Findings of Precision

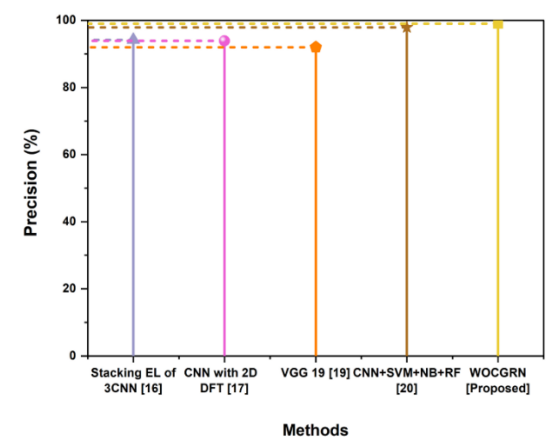| Methods	Precision (%)
Stacking EL of 3CNN [16]	94.20
CNN with 2D DFT [17]	93.08
VGG 19 [19]	92
CNN+SVM+NB+RF [20]	93.87
WOCGRN [Proposed]	**99**

Figure 9: Graphical Consequences of Precision

4.2.3 Recall

It represents the proportion of actual cataract cases correctly detected out of all real cataract cases. It measures how well the model identifies cataract cases. Research model achieves a 98.00% recall, higher than VGG 19 (96%), and Stacking EL of 3 CNN (94.89%).**Table 5** demonstrates the numerical outcomes of recall and **Figure 10** shows the graphical outcomes of recall.

Table 5: Numerical Consequences of Recall

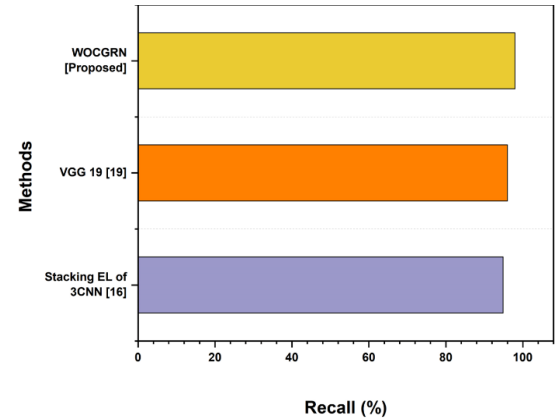| Methods	Recall (%)
Stacking EL of 3CNN [16]	94.89
VGG 19 [19]	96
WOCGRN [Proposed]	**98**

Figure 10: Graphical Outcomes of Recall

4.2.4 F1-score

It is defined as the harmonic mean of recall and accuracy, balancing both measures. It helps ensure that neither false positives nor false negatives predominate in cataract detection when both accuracy and recall are crucial. **Figure 11** depicts the graphical outcome of f1-score. WOCGRN achieves the findings of an F1-score is 98.00%, outperforming Stacking EL of 3 CNN (94.89%),CNN with 2D-DFT (93.09%), and VGG 19 (94%), as shown in **Table 6.**

Table 6: Numerical findings of F1-score

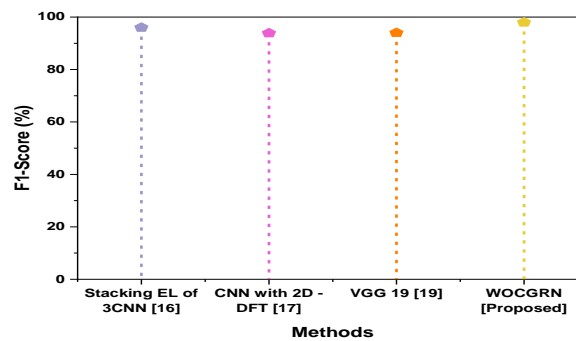| Methods	F1-Score (%)
Stacking EL of 3CNN [16]	94.89
CNN with 2D - DFT [17]	93.08
VGG 19 [19]	94
WOCGRN [Proposed]	**98**

Figure 11: Graphical outcomes of F1score

4.2.5 Sensitivity

It assesses how effectively the model detects true cataract cases, highlighting how a framework can detect every affirmative instance. **Figure 12** and **Table 7** shows the outcomes of the proposed; it achieves a 97.00% sensitivity, compared to Stacking EL of 3 CNN (95.59%), CNN with 2D - DFT (93.13%), LeNet-CNN (95%), and CNN+SVM+NB+RF (95.63%).

Table 7: Numerical Findings of Sensitivity

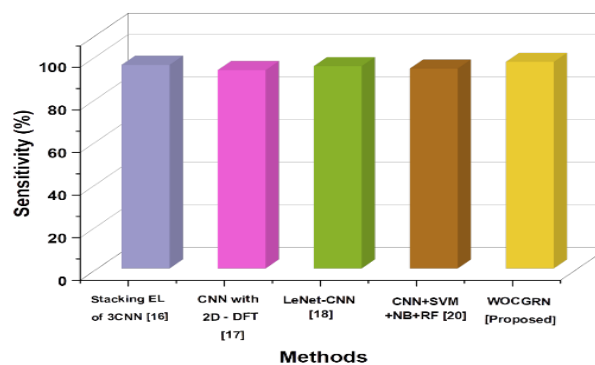| Methods	Sensitivity (%)
Stacking EL of 3CNN [16]	95.59
CNN with 2D - DFT [17]	93.13
LeNet-CNN [18]	95
CNN+SVM+NB+RF [20]	95.63
WOCGRN [Proposed]	**97**

Figure 12: Graphical results of Sensitivity

4.2.6 Specificity

It measures the proportion of non-cataract cases correctly identified out of all definite non-cataract cases. With 96.00% specificity, the WOCGRN also outperforms models like CNN+SVM+NB+RF (97.92%) and Stacking EL of 3 CNN (91.67%) in **Table 8** and **Figure 13**.

Table 8: Numerical Outcomes of Specificity

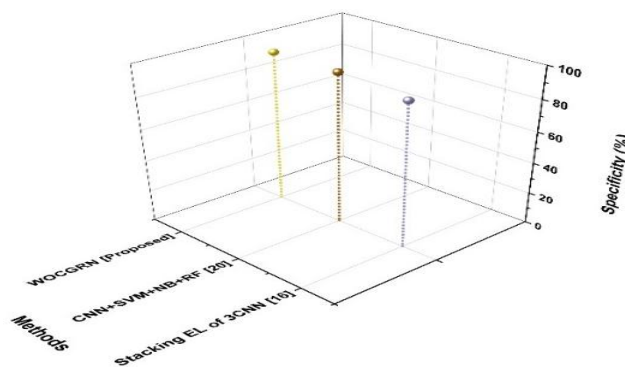| Methods	Specificity (%)
Stacking EL of 3CNN [16]	91.67
CNN+SVM+NB+RF [20]	97.92
WOCGRN [Proposed]	**96**

Figure 13: Graphical representation of Specificity

4.2.7 Confusion matrix

A confusion matrix is a table that shows the counts of true positives, true negatives, false positives, and false negatives and is used to assess how well a classification model performs. **Figure 14** displays the confusion matrix's results. The effectiveness of a classification model is displayed in this confusion matrix throughout four classes (Class 0, Class 1, Class 2, and Class 3). Class 0 was predicted correctly 109 times with no misclassifications classes. Class 1 was correctly predicted 33 times, while 14 instances of Class 1 were misclassified as Class 0, with one misclassified as Class 2. For Class 2, the model achieved 19with one misclassified as Class 3 and for Class 3, the model attained 23 correct predictions with no misclassifications classes.
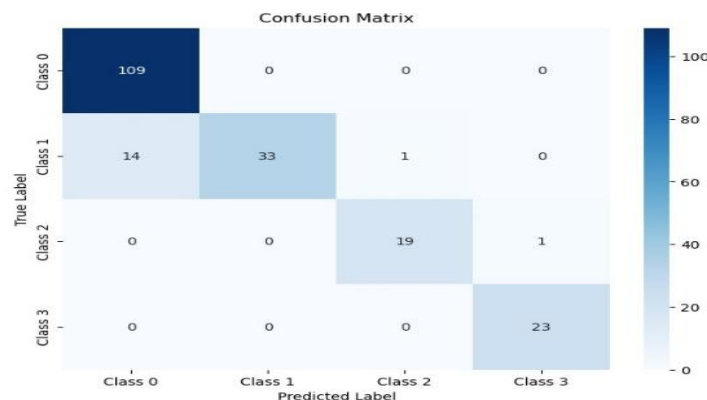

Figure 14: Confusion Matrix

4.3 Discussion

The cataract detection technique has a number of shortcomings. Its efficacy on novel situations may be diminished by overfitting the training data because to the complexity of stacking EL of 3 CNN**[16]**. CNN's reliance on feature

extraction in 2D DFT **[17]** may result in missed detections and higher processing requirements. Lower accuracy and the absence of crucial parameters like precision and recall compromise LeNet-CNN's **[18]** dependability. VGG 19 **[19]** generalizability may be compromised by overfitting and resource consumption. Finally, the CNN + SVM + NB + RF **[20]** ensemble approach is involved, computationally demanding, and may lead to increased false positive rates. By merging convolutional and recurrent layers, the WOCGRN improves cataract diagnosis by enabling better feature extraction and temporal analysis of eye images. When compared to conventional techniques, this results in increased accuracy and resilience in the identification of cataract patients.

V.   CONCLUSION

Research improves the efficiency and accuracy of cataract recognition from medical images by integrating the capabilities of GRU with CNNs. WO strategies ensure fast convergence and accurate forecasts by enhancing the performance of the model even more. By enabling early intervention and improved patient outcomes, this novel paradigm has the potential to revolutionize standard eye exams. In summary, this method represents a positive advancement in the use of artificial intelligence (AI) for cataract early diagnosis. The proposed WOCGRN model demonstrates significantly higher performance metrics, achieving **99.49%** accuracy, **99.00%** precision, **98.00%** recall, **98.00%** F1 score, **97%** sensitivity, and **96%** specificity compared to existing models.

Drawbacks and future scope: The WOCGRN has the potential for early cataract diagnosis, but its limited resource effectiveness can hinder its application. Future research should focus on model resilience and transfer learning strategies.

REFERENCES

[1]   Lim, J.C., Jiang, L., Lust, N.G. and Donaldson, P.J., 2024. Minimizing Oxidative Stress in the Lens: Alternative Measures for Elevating Glutathione in the Lens to Protect against Cataract. *Antioxidants*, *13*(10), p.1193. https://doi.org/10.3390/antiox13101193

[2]   Abazaga, M. and Fechtner, R., 2024. Changes and Diseases of the Aging Eye. In *Geriatric Medicine: A Person Centered Evidence Based Approach* (pp. 663689). Cham: Springer International Publishing.https://doi.org/10.1007/978 3 030 74720 6_58

[3]   Vergroesen, J.E., Thee, E.F., Ahmadizar, F., van Duijn, C.M., Stricker, B.H., Kavousi, M., Klaver, C.C. and Ramdas, W.D., 2022. Association of diabetes medication with open-angle glaucoma, age-related macular degeneration, and cataract in the Rotterdam study. *JAMA ophthalmology*, *140*(7), pp.674-681.https://doi.org/10.1001/jamaophthalmol.2022.1435

[4]   Cvekl, A. and Vijg, J., 2024. Aging of the eye: Lessons from cataracts and agerelated macular degeneration. *Ageing Research Reviews*, p.102407. https://doi.org/10.1016/j.arr.2024.102407

[5]   Shiels, A. and Hejtmancik, J.F., 2021. Inherited cataracts: Genetic mechanisms and pathways new and old. *Experimental eye research*, *209*, p.108662.https://doi.org/10.1016/j.exer.2021.108662

[6]   Hsiu Hung, Y. and Zi Lin, W., 2024. Vision Problems and Eyewear Design Opportunities for the Elderly. https://doi.org/10.21606/drs.2024.326

[7]   Karimi, A., Stanik, A., Kozitza, C. and Chen, A., 2024. Integrating Deep Learning with Electronic Health Records for Early Glaucoma Detection: A Multi-Dimensional Machine Learning Approach. *Bioengineering*, *11*(6), p.577.https://doi.org/10.3390/bioengineering11060577

[8]   Mohammad, N.K., Rajab, I.A., Al-Taie, R.H. and Ismail, M., 2024. Machine Learning and Vision: Advancing the Frontiers of Diabetic Cataract Management. Cureus, 16(8).https://doi.org/10.7759%2Fcureus.66600

[9]   Saqib, S.M., Iqbal, M., Asghar, M.Z., Mazhar, T., Almogren, A., Rehman, A.U. and Hamam, H., 2024. Cataract and glaucoma detection based on Transfer Learning using MobileNet. *Heliyon*, *10*(17).https://doi.org/10.1016/j.heliyon.2024.e36759

[10]   Zannah, T.B., AbdullaHilKafi, M., Sheakh, M.A., Hasan, M.Z., Shuva, T.F., Bhuiyan, T., Rahman, M.T., Khan, R.T., Kaiser, M.S. and Whaiduzzaman, M., 2024. Bayesian Optimized Machine Learning Model for Automated Eye Disease Classification from Fundus Images. *Computation*, *12*(9), p.190.https://doi.org/10.3390/computation12090190

[11]   Ibrahim, A., Sabara, E., Dirsam, W. and Aziz, F., 2024. Optimising Cataract Detection in Fundus Images through EfficientNetBased Classification. *Journal Medical Informatics Technology*, pp.15. https://doi.org/10.37034/medinftech.v2i1.25

[12]   A Jabber, A., Hassan Hadi, A. and Muhsin Wadi, S., 2024. Cataract Detection and Classification Using Deep Learning Techniques. *International Journal of Computing and Digital Systems*, *16*(1), pp.110. http://dx.doi.org/10.12785/ijcds/XXXXXX

[13]   Tan, Y., Zou, Y.S., Yu, Y.L., Hu, L.Y., Zhang, T., Chen, H., Jin, L., Lin, D.R., Liu, Y.Z., Lin, H.T. and Liu, Z.Z., 2024. Classification of congenital cataracts based on multidimensional phenotypes and its association with visual outcomes. *International Journal of Ophthalmology*, *17*(3), p.473. https://doi.org/10.18240%2Fijo.2024.03.08

[14]   Hermadiputri, F.Y., Mandyartha, E.P. and Rizki, A.M., 2024. Implementation Of Support Vector Machine And Harmony Search For Cataract Severity Classification In Fundus Images. *JurnalSistemInformasidanIlmuKomputer*, *8*(1), pp.2941. https://doi.org/10.34012/jurnalsisteminformasidanilmukomputer.v8i1.5394

[15]   Gao, W., Shao, L., Li, F., Dong, L., Zhang, C., Deng, Z., Qin, P., Wei, W. and Ma, L., 2024. Fundus photographbased cataract evaluation network using deep learning. *Frontiers in Physics*, *11*, p.1235856.https://doi.org/10.3389/fphy.2023.1235856

[16]   Elloumi, Y., 2022. Cataract grading method based on deep convolutional neural networks and stacking ensemble learning. *International Journal of Imaging Systems and Technology*, *32*(3), pp.798814.https://doi.org/10.1002/ima.22722

[17]   Yadav, S. and Yadav, J.K.P.S., 2023. Automatic Cataract Severity Detection and Grading Using Deep Learning. *Journal of Sensors*, *2023*(1), p.2973836. https://doi.org/10.1155/2023/2973836

[18]   Ganokratanaa, T., Ketcham, M. and Pramkeaw, P., 2023. Advancements in Cataract Detection: The Systematic Development of LeNet-Convolutional Neural Network Models. Journal of Imaging, 9(10), p.197.https://doi.org/10.3390/jimaging9100197

[19]   Muchibwa, C., Eldaw, M.H.S., Mu Mu and Agyeman, M.O., 2024. An Assessment of Contemporary Methods and Data-Enabled Approaches for Early Cataract Detection. *F1000Research*, *12*, p.998.https://doi.org/10.12688/f1000research.138294.2

[20]   Yadav, S. and Yadav, J.K.P.S., 2023. Enhancing cataract detection precision: A deep learning approach. *Traitement du Signal*, *40*(4), p.1413.https://doi.org/10.18280/ts.400410